

Article

Double Notched Long-Period Fiber Grating Characterization for CO₂ Gas Sensing Applications [†]

Hsiang-Chang Hsu, Tso-Sheng Hsieh, Tzu-Hsuan Huang, Liren Tsai and Chia-Chin Chiang * 

Department of Mechanical Engineering, National Kaohsiung University of Sciences and Technology, NO. 415 Jian-gong Road, Kaohsiung, Kaohsiung City 80778, Taiwan; gn1204774@gmail.com (H.-C.H.); srcx2s904@gmail.com (T.-S.H.); iamjohnny825@gmail.com (T.-H.H.); liren@nkust.edu.tw (L.T.)

* Correspondence: ccchiang@kuas.edu.tw; Tel.: +886-7381-4526-5340

[†] This paper is an extended version of Hsiang-Chang Hsu, Tso-Sheng Hsieh, Chia-Chin Chiang's paper "Investigation on high temperature characteristics of metal-coated FBG sensors" published in proceedings of the 6th International Symposium on Sensor Science (I3S 2018), Kenting, Taiwan, 6–8 August 2018.

Received: 24 August 2018; Accepted: 20 September 2018; Published: 22 September 2018



Abstract: In this study, we applied a double-sided inductively coupled plasma (ICP) process to nanostructure long-period fiber grating (LPFG) in order to fabricate a double-notched LPFG (DNLPG) sensor with a double-sided surface corrugated periodic grating. Using the sol-gel method, we also added thymol blue and ZnO to form a gas sensing layer, thus producing a DNLPG CO₂ gas sensor. The resulting sensor is the first double-sided etching sensor used to measure CO₂. The experimental results showed that as the CO₂ concentration increased, the transmission loss increased, and that the smaller the fiber diameter, the greater the sensitivity and the greater the change in transmission loss. When the diameter of the fiber was 32 μm (and the period was 570 μm) and the perfusion rate of CO₂ gas was 15%, the maximum loss variation of up to 3.881 dB was achieved, while the sensitivity was 0.2146 dB/% and the linearity was 0.992. These results demonstrate that the DNLPG CO₂ gas sensor is highly sensitive.

Keywords: sol-gel; CO₂; gas sensor

1. Introduction

In recent years, optical fiber has been utilized in an extensive range of applications due to its light weight, immunity to electro-magnetic interference, low power consumption, corrosion resistance, and high temperature resistance [1]. Among the different types of optical fiber, long-period fiber grating (LPFG) has been widely used in the fields of optical communication and sensing systems [2]. LPFG consists of periodic refractive index variations with periods from about 100 μm to 1 mm. The attenuation dip of LPFG is sensitive to environmental parameters and thus can be used to measure and monitor changes in physical parameters. That is, it can be used as an optical fiber sensor.

The processes used to manufacture different types of LPFG include excimer laser writing [3], CO₂ laser-induced writing [4], the arc discharge technique [5], the mechanical pressure method [6], polyelectrolyte multilayer (PEM) coating [7], and the use of micro-electromechanical systems technology for etching and the application of photoresist [8]. Furthermore, the inductively coupled plasma (ICP) etching technique has been used to fabricate notched LPFG (NLPFG) with a dry etch barrier [9]. In this study, we used the ICP method to fabricate a double NLPFG (DNLPG) CO₂ gas sensor. CO₂ accounts for only 4% of the atmosphere, but the increasing volumes of the CO₂ in the atmosphere have a major impact on global warming [10]. Therefore, it is important to detect and control the emission of CO₂ into the atmosphere. In addition, high concentrations of CO₂ can cause poisoning, and even lead to convulsions, coma, and death [11]. As such, the detection of CO₂

is a topic very worthy of in-depth study. The existing types of CO₂ sensors can be divided into semiconductor sensors [12], chemical sensors [13], optical fiber sensors [14], laser diode sensors [15], and non-dispersive infrared (NDIR) sensors [16]. Among those different types, NDIR sensors have been widely employed. However, NDIR sensors have a variety of limitations, such as being bulky and high in cost.

Therefore, some scholars have begun to study the option of coating a sensing layer on an optical fiber to serve as a CO₂ sensor. For example, Segawa et al. [17] used the sol-gel method to coat thymol blue on optic fiber in order to measure CO₂ concentrations, finding that the maximum transmission loss variation for their sensor was 2.08 dB, while its sensitivity was about 0.112 dB/%. In contrast, James et al. [18] used pentavinyll hexylamine to sense CO₂, finding that the maximum transmission loss variation for their sensor was 2.49 dB, while its sensitivity was approximately 0.0727 dB/%. Meanwhile, Wu et al. [19] used NLPFG with an amine-modified surface nanostructure to measure CO₂, finding that the maximum transmission loss variation for their sensor was 2.019 dB, while its sensitivity was approximately 0.089 dB/%.

In this study, we used the sol-gel method [20] to mix thymol blue with ZnO and then coated that mixture on DNLPFG to create a CO₂ sensor that is small in size, easy to manufacture, easy to carry, and low in cost.

2. Working Principle

The transmission loss of light through LPFG is defined [21] as

$$T = \frac{1}{1 + \frac{k^{dc}}{k_{co-cl}^{ac}}} \cos^2 \left(\sqrt{\left(k_{co-cl}^{ac}\right)^2 + \left(k^{dc}\right)^2} L \right) \quad (1)$$

where k^{dc} , k_{co-co}^{dc} , and k_{cl-cl}^{dc} are all LPFG coupling coefficients, k_{co-cl}^{ac} is an AC coupling coefficient, and $k^{dc} = k_{co-co}^{dc} = k_{cl-cl}^{dc} = 0$. Thus, Equation (1) can be simplified to

$$T = \cos^2 \left(k_{co-cl}^{ac} L \right). \quad (2)$$

The transmission loss of light through LPFG is a cosine squared function, where the transmission loss is dependent on the coupling coefficients and the length of the grating. The combination of CO₂ gas and sol-gel mix with the thymol blue and nano-ZnO sensing layer changes the effective refractive index for the cladding in Equation (2), thus affecting the coupling coefficient $\left(k_{co-cl}^{ac}\right)$, such that when the gas is detected, the coupling coefficients for the cladding and core become smaller, decreasing the transmission loss. Inputting the experimental data into Equation (2) allows the changes in loss to be determined.

3. Manufacturing Process and Experiment Setup

3.1. DNLPFG Gas Sensor Manufacturing Process

In this study, the double-sided ICP process was applied to single-mode optical fibers (Corning SMF28e) in order to fabricate the DNLPFG sensor with a double-sided surface corrugated periodic grating. This DNLPFG sensor fabrication process is shown in Figure 1. A buffer oxide etch (BOE) chemical was used on the etched fibers to reduce the diameter from 125 to 40, 35, or 32 μm. The fibers were then connected into two metal grating masks (i.e., amplitude masks), and an ICP-etcher was used to generate the double-sided surface corrugated periodic grating of the DNLPFG. Finally, the DNLPFG was obtained after the etched device was released from the metal mask. An SEM image of the DNLPFG sensor is shown in Figure 2.

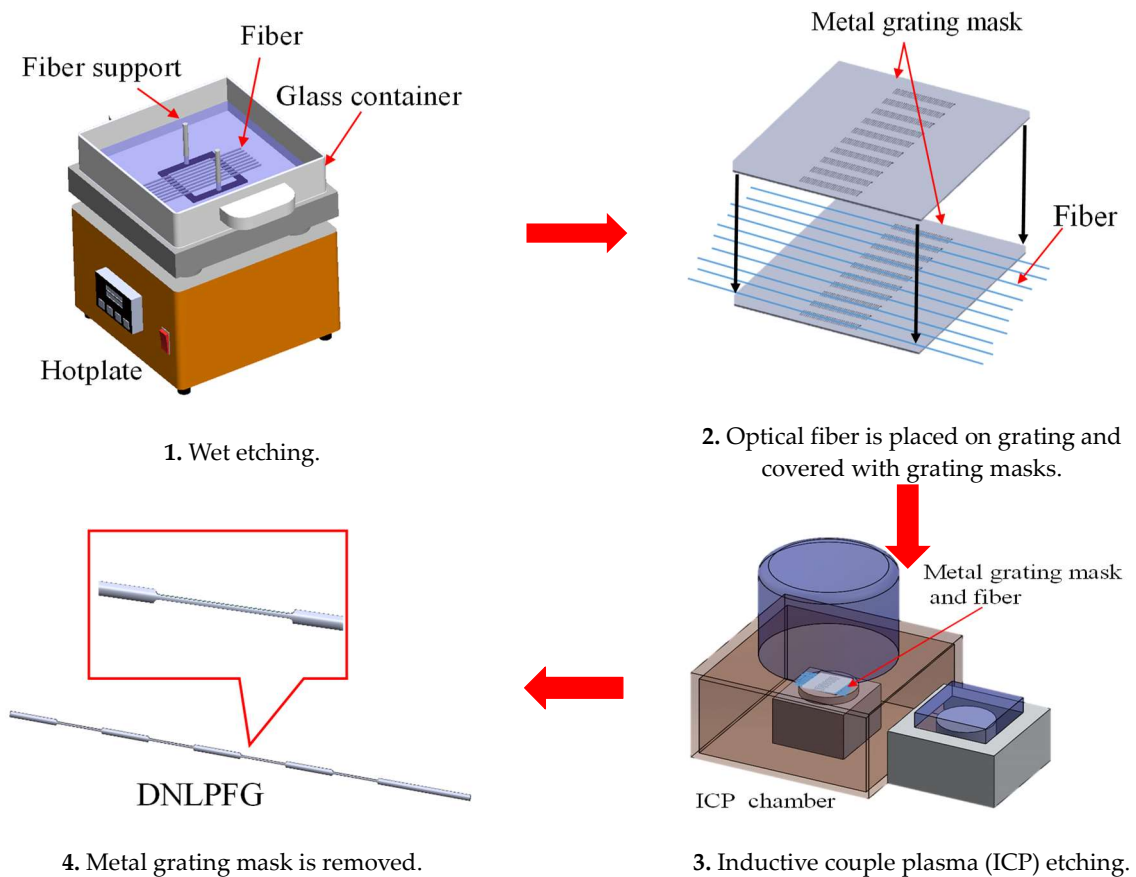


Figure 1. Double-notched long-period fiber grating (DNLPG) manufacturing process.

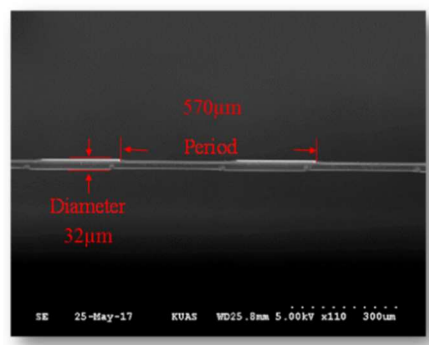


Figure 2. DNLPG SEM image.

3.2. Sol-Gel Coated DNLPG CO₂ Gas Sensor Process

The two different nanoparticles of thymol blue and ZnO were used with a sol-gel to make a gas sensing layer. Tetraethoxysilane (TEOS) (4 mL) and *n*-octyltriethoxysilane (Octyl-triEOS) (0.2 mL) were mixed in proportion and then added to and mixed with anhydrous EtOH (1 mL) and hydrochloric acid (HCl) (0.4 mL) to make the sol-gel. The solution was then capped and magnetically stirred for 1 h at room temperature. At this stage, Triton-X-100 (0.1 mL) was added to improve the homogeneity of the silica sol, resulting in a crack-free monolith.

The optic fiber CO₂ sensor developed in this study was based on a sol-gel matrix composed of organically modified silica (ORMOSIL) doped with thymol blue, ZnO, or a mix of thymol blue with ZnO nanoparticles to create three different sensing layers, here the ratio of the mixture is 1:1 in volume. The solutions were then draped on the DNLPG sensor to form a gas sensing layer, as shown in Figure 3. An SEM image of the sol-gel coated DNLPG sensor is shown in Figure 4.

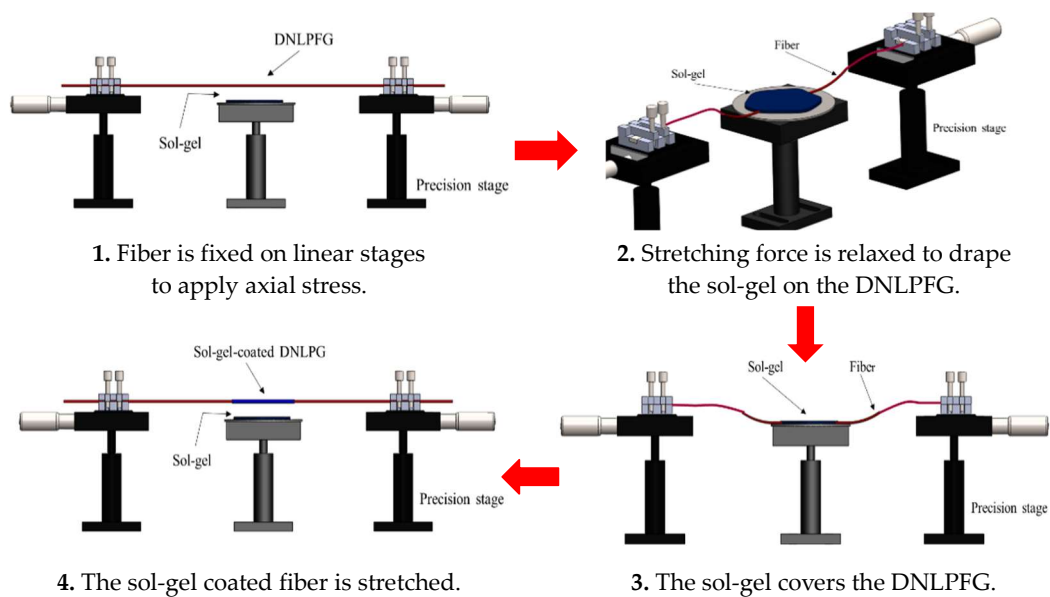


Figure 3. Production flow chart of sol-gel coated DNLPG sensor.

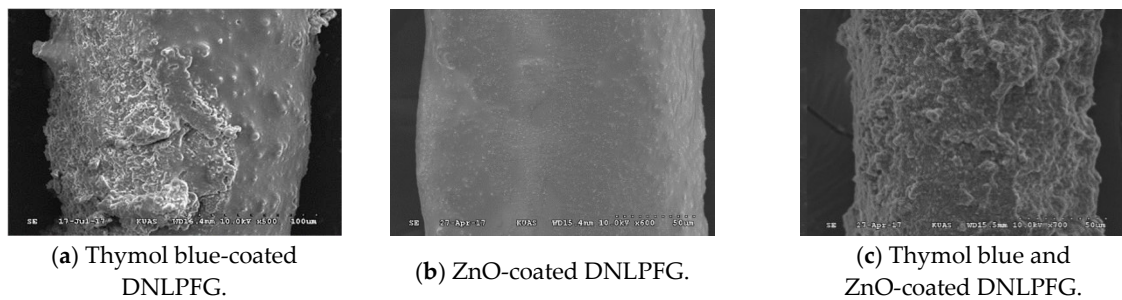


Figure 4. Sol-gel coated DNLPG CO₂ gas sensor SEM images.

3.3. Packaging of DNLPG CO₂ Gas Sensor

The spectra of a DNLPG (with a diameter of 32 μm and period of 570 μm) deform under increased loading, as shown in Figure 5, while the resonant dip of the DNLPG intensifies with increased loading. When the force loading increases from 0 to 0.0343 N, the resonant dip loss changes from -1.55 to -15.02 dB, and then when the loading increases from 0.0343 to 0.0441 N, this resonant dip loss changes from -15.02 to -11.31 dB. The maximum resonant dip of the DNLPG sensor was thus -15.02 dB, and the resonant wavelength was 1541.35 nm under 0.0343 N loading. Since the cross section of core of the DNLFBG is small, the applied force to stretch the sensor is small as well. The stretch will make the sensor more sensible. So that, the external axial stress was applied to the sol-gel coated DNLPG gas sensor, it will produce transmission loss for the gas sensing experiments. Because the load element and micro-motion platform to fix the stretching force is inconvenient and difficult to use outdoors, we kept the sensor stretched and fixed on the stage and sleeved with a U-shaped quartz tube, UV glue was then dropped on both ends of the quartz tube. Finally, the UV light was irradiated on the UV glue to package the sensor in a U-shaped quartz tube (shown as Figure 6) The sensor after the package does not required load cell and micro-motion platform, can reduce the experimental equipment, easy to place in the gas experiment chamber.

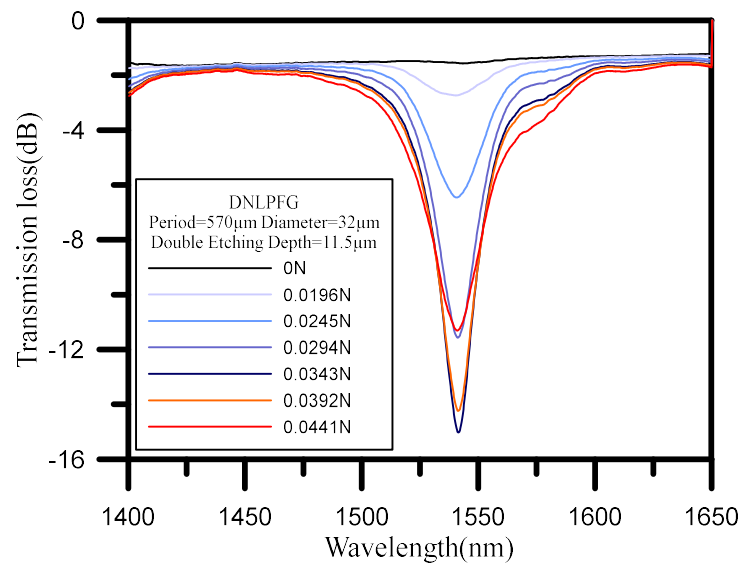


Figure 5. The transmission spectra of DNLPGF sensor under tensile loading.

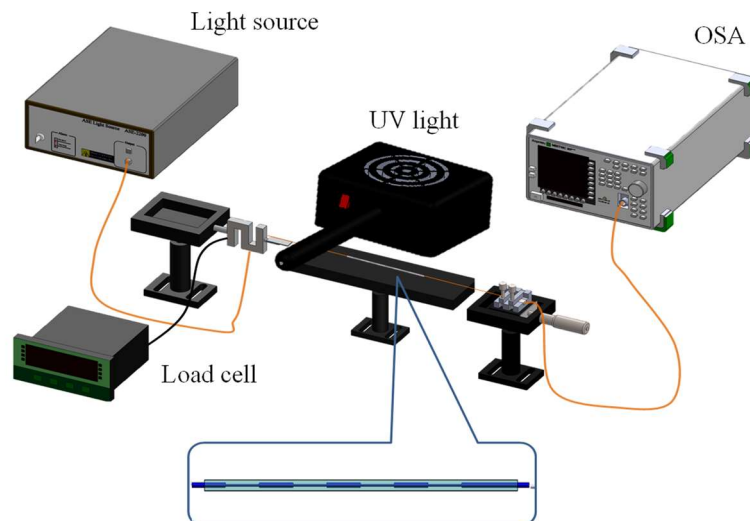


Figure 6. Schematic diagram for packaging of DNLPGF CO₂ gas sensor.

3.4. The Experimental Setup of CO₂ Gas Sensing

Figure 7 shows the sol-gel coated DNLPGF CO₂ gas sensor experimental setup. The sol-gel coated DNLPGF sensor was sealed inside of a U-shaped quartz tube which was in turn placed inside of a gas sensor chamber fitted with a gas loading and unloading system. A gas mixer adjusted the concentration of the CO₂ gas for experiments using different concentrations of CO₂. A spectrometer was used to observe the changes in the DNLPGF sensor spectrum after different concentrations of CO₂ were introduced for analysis.

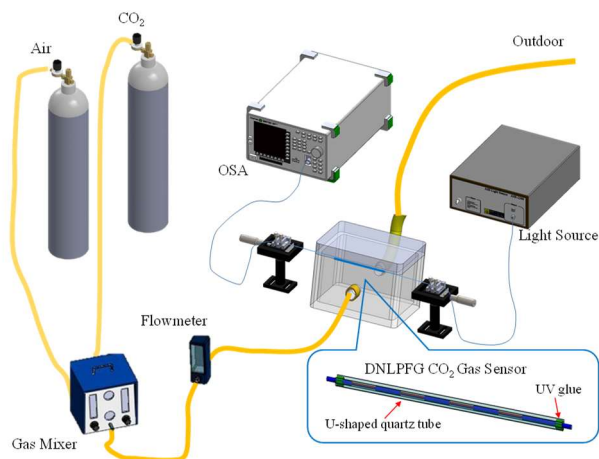


Figure 7. The experimental setup of CO₂ gas sensing with the sol-gel coated DNLPG CO₂ gas sensor.

4. Results and Discussion

4.1. Response Sensitivity Characteristics of CO₂ Gas Sensing with Different Sensing Films

A DNLPG sensor with a diameter of 40 μm and period of 600 μm was used in this experiment. The optic fiber CO₂ sensor developed in this study was based on a sol-gel matrix composed of ORMOSIL doped with thymol blue, ZnO, or a mix of thymol blue with ZnO nanoparticles to create three different sensing film layers. A spectrometer was used to observe the changes in the DNLPG sensor spectrum after concentrations of 15% CO₂ were introduced for 15 min.

Figure 8 shows the changes in transmission loss for the CO₂ gas sensor with different sensing films. The figure shows that in the five cyclic experiments, the sensing film layer consisting of a mix of thymol blue with ZnO had the largest transmission loss (1.958–2.257 dB), the sensing film layer consisting of a thymol blue had the second largest transmission loss (1.678–1.765 dB), and the sensing film layer consisting of ZnO had the smallest transmission loss (0.366–0.787 dB). The best response sensitivity setting was for the DNLPG coated with a film of sol-gel matrix composed of ORMOSIL doped with a mix of thymol blue and ZnO.

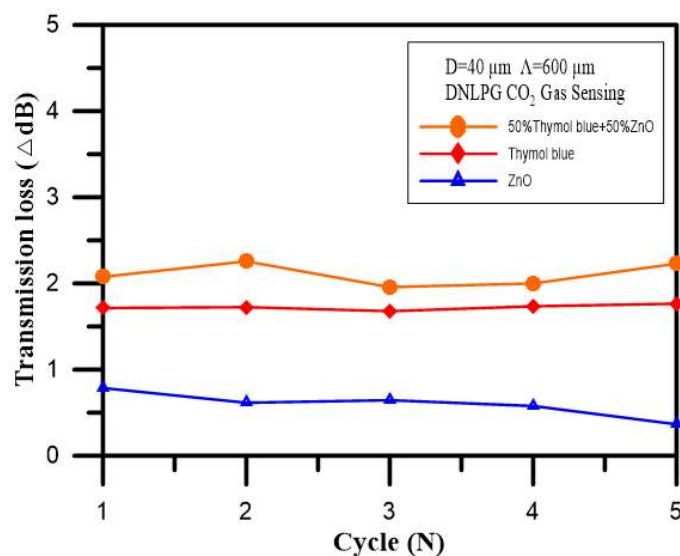


Figure 8. Changes in transmission loss for the CO₂ gas sensors with different sensing films.

4.2. Response Sensitivity Characteristics of CO₂ Gas Sensors with Different Diameters

It had been learned from the previous experiment that the DNLPG coated with the sol-gel mixed with thymol blue solution doped with a mix of thymol blue with ZnO was very effective in terms of CO₂ gas sensing. The next step was to explore the effects of changes in diameter by measuring CO₂ using different fiber's diameters, which would affect the amount of change in transmission loss, sensitivity, and reproducibility. The sensing layer was coated with a sol-gel mixture of thymol blue and zinc oxide. Three DNLPG sensors with diameters of 40 μm (period of 600 μm), 35 μm (period of 580 μm), and 32 μm (period of 570 μm), respectively, were used in this experiment. The period is calculated referring to the equation in the literature [22].

Figure 9 shows the changes in transmission loss for these CO₂ gas sensors with different diameters. The figure shows that in the five cyclic experiments for the three types DNLPG, the DNLPG sensor with a diameter of 32 μm had the largest transmission loss (3.762–3.881 dB), the DNLPG sensor with a diameter of 35 μm had the second largest transmission loss (2.793–2.996 dB), and the DNLPG sensor with a diameter of 40 μm had the smallest transmission loss (1.958–2.257 dB). The best response sensitivity was observed for the DNLPG with a diameter of 32 μm (period of 570 μm) coated with a sol-gel mixture of thymol blue and zinc oxide. Additionally, a small stretching force was required for the sensor to obtain higher sensitivity.

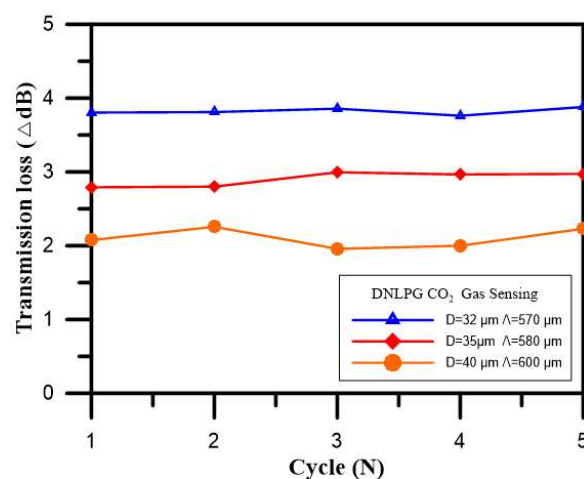


Figure 9. Changes in transmission loss for the CO₂ gas sensors with different diameters.

4.3. CO₂ Gas Concentration Robust Sensing Experiment

For this experiment, we used the 32 μm diameter, 570 μm period optic fiber coated with a sol-gel mixture of thymol blue and zinc oxide and then completely sealed in a box. An initial load of nitrogen was input into the box until the CO₂ gas sensor spectrum was stable. Next, CO₂ was introduced into the box at a concentration of 15% for 15 min, and the spectral changes were recorded, after which air was introduced to the box for 5 min to allow the sensor to recover and stabilize. Next, CO₂ was introduced into the box at a concentration of 12% for 15 min, during which the spectral changes were recorded, and after which air was introduced to the box for 5 min to allow the sensor to recover and stabilize. This procedure was then repeated for CO₂ concentrations of 9%, 6%, and 3%. Figure 10 shows the changes in loss for the 15%, 12%, 9%, 6%, and 3% CO₂ gas concentrations sensed in three cyclic experiments. In Figure 11, we can clearly see the intensity and transmission loss variations of different concentrations of CO₂ in the three cyclic. As indicated, we found that when the gas was detected, the coupling coefficients for the cladding and core became smaller, decreasing the transmission loss, which could be verified using Equation (2). Figure 12 shows the repeatability of the CO₂ gas sensor spectral analysis. The mean and standard deviation changes in transmission loss for CO₂ at concentrations of 15%, 12%, 9%, 6%, and 3% were 3.7673 dB, 3.0077 dB, 2.3400 dB, 1.6683dB, and 1.2180 dB (as shown in

Table 1), respectively. As the CO₂ concentration increased, the transmission loss increased; sensitivity was 0.2146 dB/% and linearity was 0.992.

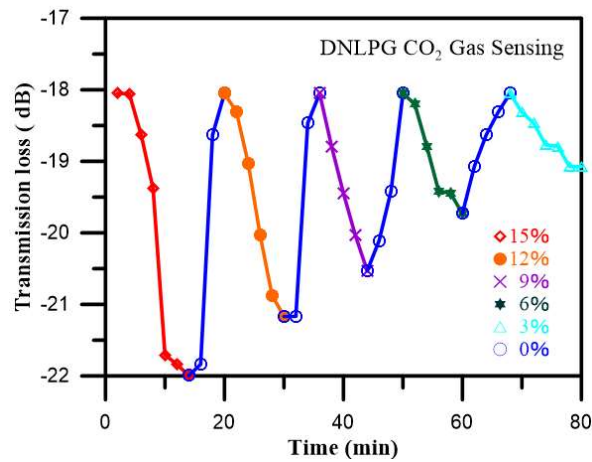


Figure 10. The online monitoring diagram of the 15%, 12%, 9%, 6%, and 3% CO₂ gas concentrations over three cyclic experiments.

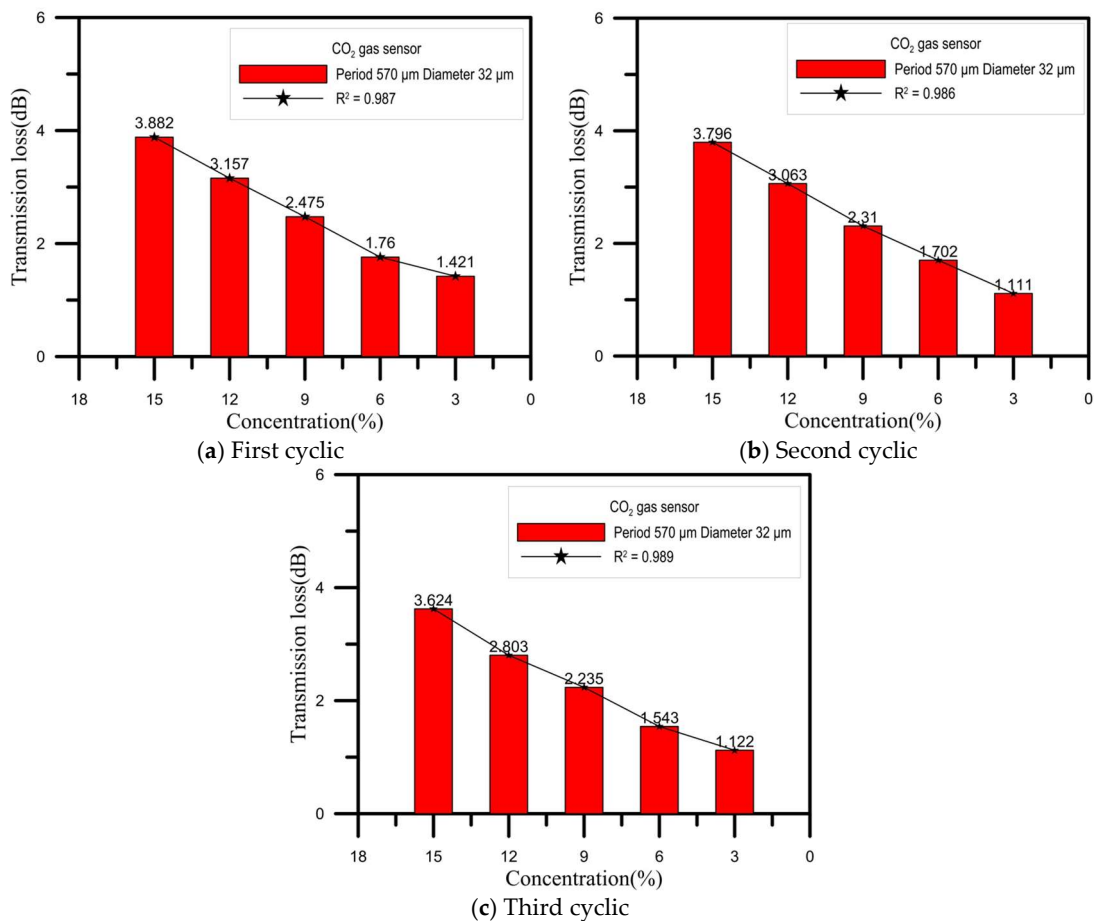


Figure 11. Response characteristics of sensing for the 15%, 12%, 9%, 6%, and 3% CO₂ gas concentrations over three cyclic experiments. (a) First cyclic; (b) second cyclic; (c) third cyclic.

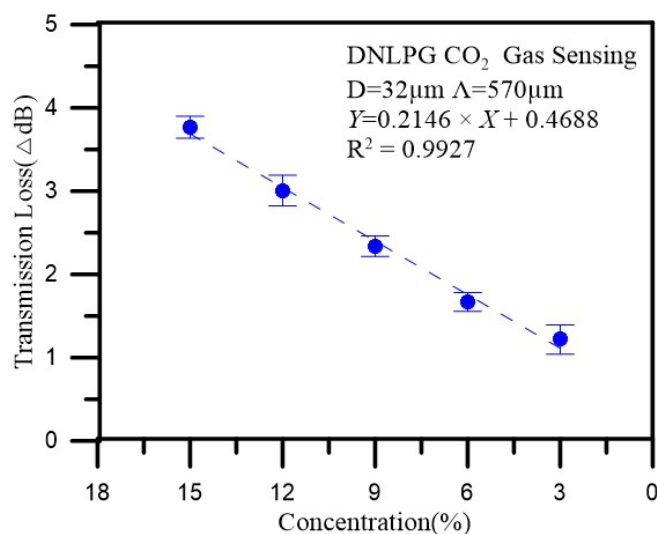


Figure 12. Repeatability of the CO₂ gas sensor spectral analysis.

Table 1. Mean and standard deviation changes in loss for the different CO₂ gas concentrations.

CO ₂ Concentration	Mean Loss (dB)	Standard Deviation of Loss (dB)
15%	3.7673	0.1313
12%	3.0077	0.1833
9%	2.3400	0.1227
6%	1.6683	0.1123
3%	1.2180	0.1758

According to the literature [17–19], the maximum transmission loss variation of previously reported sensors was 2.50 dB, while the associated sensitivity was approximately 0.089 dB/% (as shown in Table 2). In this study, in which we coated DNLPG with thymol blue mixed with ZnO, the maximum transmission loss variation was 3.881 dB and the sensitivity was approximately 0.2146 dB/%. The maximum transmission loss variation and the sensitivity were thus 56% ($|3.881 - 2.50|/2.50$) and 141% ($|0.2146 - 0.089|/0.089$) higher, respectively, than those for the best sensors previously reported in the literature.

Table 2. Comparison with different sensors used to measure CO₂ concentrations.

Ref.	Sensing Film	Concentration	Transmission Loss Variation	Sensitivity
[17]	Thymol blue	0–100%	2.500 dB	0.0250 dB/%
[18]	PEHA	0–15%	2.490 dB	0.0727 dB/%
[19]	TEPA	0–15%	2.019 dB	0.0890 dB/%
In this study	Thymol blue ZnO	0–15%	3.881 dB	0.2146 dB/%

5. Conclusions

This study used DNLPG gas sensors with diameters of 40, 35, and 32 μm, respectively, and coated them with a mix of thymol blue and ZnO as a sensing layer using the sol-gel method to detect 3% to 15% concentrations of CO₂ gas. When the diameter of the fiber was 32 μm (and the period was 570 μm) and the CO₂ gas concentration reached 15%, the results showed that the maximum loss variation reached up to 3.881 dB, while the sensitivity was 0.2146 dB/% and the linearity was 0.992. This maximum transmission loss and sensitivity were thus 56% and 141% better, respectively, than those for the best sensors previously reported in the literature. These results demonstrate that the DNLPG CO₂ gas sensor is quite sensitive in terms of detecting CO₂ at room temperature.

Author Contributions: Writing-Original Draft, H.-C.H., T.-S.H. and T.-H.H.; Writing-Review & Editing, L.T. and C.-C.C.

Funding: This work was supported by the Ministry of Science and Technology, Taiwan (grant number MOST 107-2221-E-992-043-MY3).

Conflicts of Interest: The authors declare no conflict of interest.

References

1. Hong, C.-Y.; Zhang, Y.-F.; Zhang, M.-X.; Leung, L.M.G.; Liu, L.-Q. Application of FBG sensors for geotechnical health monitoring, a review of sensor design, implementation methods and packaging techniques. *Sens. Actuators A Phys.* **2016**, *244*, 184–197. [[CrossRef](#)]
2. Kheiri, M.; Zibaii, M.; Sadeghi, J.; Latifi, H. Refractive index measurement by fat long period grating sensor on a single mode optical fiber. In Proceedings of the Asia Communications and Photonics Conference and Exhibition (ACP), Shanghai, China, 13–16 November 2011.
3. Libish, T.M.; Bobby, M.C.; Linesh, J.; Mathew, S.; Biswas, P.; Bandyopadhyay, S.; Dasgupta, K.; Radhakrishnan, P. The effect of annealing and temperature on transmission spectra of long period gratings written in hydrogen loaded standard single mode fiber. *Optik* **2013**, *124*, 4345–4348. [[CrossRef](#)]
4. Wang, B.; Zhang, W.; Bai, Z.; Wang, L.; Zhang, L.; Zhou, Q.; Chen, L.; Yan, T. CO₂-Laser-induced long period fiber gratings in few mode fibers. *IEEE Photonics Technol. Lett.* **2015**, *27*, 145–148. [[CrossRef](#)]
5. Yin, G.; Wang, Y.; Liao, C.; Zhou, J.; Zhong, X.; Liu, S.; Wang, Q.; Li, Z.; Sun, B.; He, J.; et al. Improved arc discharge technique for inscribing compact long period fiber gratings. In Proceedings of the 23rd International Conference on Optical Fiber Sensors, Santander, Spain, 2–9 June 2014.
6. Tsutsumi, Y.; Ohashi, M.; Miyoshi, Y. Temperature-sensitive mechanical LPFG using contractive force of heat-shrinkable tube. *Opt. Fiber Technol.* **2013**, *19*, 55–59. [[CrossRef](#)]
7. Li, Q.S.; Zhang, X.L.; He, H.; Meng, Q.J.; Shi, J.G.; Wang, J.N.; Dong, W.F. Improved detecting sensitivity of long period fiber gratings by polyelectrolyte multilayers: The effect of film structures. *Opt. Commun.* **2014**, *331*, 39–44. [[CrossRef](#)]
8. Chiang, C.C.; Cheng, T.C.; Chang, H.J.; Tsai, L. Sandwiched long-period fiber grating filter based on periodic SU8-thick photoresist technique. *Opt. Lett.* **2009**, *34*, 3677–3679. [[CrossRef](#)] [[PubMed](#)]
9. Chiang, C.C.; Tsai, L. Perfectly notched long-period fiber grating filter based on ICP dry etching technique. *Opt. Lett.* **2012**, *37*, 193–195. [[CrossRef](#)] [[PubMed](#)]
10. MacDougall, A.H.; Friedlingstein, P. The origin and limits of the near proportionality between climate warming and cumulative CO₂ emissions. *J. Clim.* **2015**, *28*, 4217–4230. [[CrossRef](#)]
11. Langford, N.J. Carbon dioxide poisoning. *Toxicol. Rev.* **2005**, *24*, 229–235. [[CrossRef](#)] [[PubMed](#)]
12. Fine, G.F.; Cavanagh, L.M.; Afonja, A.; Binions, R. Metal oxide semi-conductor gas sensors in environmental monitoring. *Sensors* **2010**, *10*, 5469–5502. [[CrossRef](#)] [[PubMed](#)]
13. Jiao, Z.; Chen, F.; Su, R.; Huang, X.; Liu, W.; Liu, J. Study on the characteristics of Ag doped CuO-BaTiO₃ CO₂ sensors. *Sensors* **2002**, *2*, 366–373. [[CrossRef](#)]
14. Chu, C.S.; Lo, Y.L. Fiber-optic carbon dioxide sensor based on fluorinated xerogels doped with HPTS. *Sens. Actuators B Chem.* **2008**, *129*, 120–125. [[CrossRef](#)]
15. Asakawa, T.; Kanno, N.; Tonokura, K. Diode laser detection of greenhouse gases in the near-infrared region by wavelength modulation spectroscopy: Pressure dependence of the detection sensitivity. *Sensors* **2010**, *10*, 4686–4699. [[CrossRef](#)] [[PubMed](#)]
16. Gibson, D.; MacGregor, C. A novel solid state non-dispersive infrared CO₂ gas sensor compatible with wireless and portable deployment. *Sensors* **2013**, *13*, 7079–7103. [[CrossRef](#)] [[PubMed](#)]
17. Segawa, H.; Ohnishi, E.; Arai, Y.; Yoshida, K. Sensitivity of fiber-optic carbon dioxide sensors utilizing indicator dye. *Sens. Actuators B Chem.* **2003**, *94*, 276–281. [[CrossRef](#)]
18. James, S.W.; Tatam, R.P. Optical fibre long-period grating sensors: Characteristics and application. *Meas. Sci. Technol.* **2003**, *14*, R49–R61. [[CrossRef](#)]
19. Wu, J.W.; Chiang, C.C. Notched Long-Period Fiber Grating with an Amine-Modified Surface Nanostructure for Carbon Dioxide Gas Sensing. *Materials* **2015**, *8*, 4535–4543. [[CrossRef](#)] [[PubMed](#)]
20. Chu, C.S.; Lo, Y.L. Highly sensitive and linear optical fiber carbon dioxide sensor based on sol-gel matrix doped with silica particles and HPTS. *Sens. Actuators B Chem.* **2009**, *143*, 205–210. [[CrossRef](#)]

21. Lin, C.Y.; Wang, L.A.; Chern, G. Corrugated long-period fiber gratings as strain, torsion, and bending sensors. *J. Lightw. Technol.* **2001**, *19*, 1159–1168.
22. Chiang, C.C.; Tseng, C.C. Characterization of notched long-period fiber gratings: effects of periods, cladding thicknesses, and etching depths. *Appl. Opt.* **2014**, *53*, 4398–4404. [[CrossRef](#)] [[PubMed](#)]



© 2018 by the authors. Licensee MDPI, Basel, Switzerland. This article is an open access article distributed under the terms and conditions of the Creative Commons Attribution (CC BY) license (<http://creativecommons.org/licenses/by/4.0/>).